Silicon (2023) 15:143–151
https://doi.org/10.1007/s12633-022-02009-7

ORIGINAL PAPER

Study of Optical Properties of Single and Double Layered Amorphous Silicon Nitride Films for Photovoltaics Applications

Pariksha Malik[1] · Harsh Gupta[1] · Santanu Ghosh[1] · Pankaj Srivastava[1]

Received: 14 February 2022 / Accepted: 1 July 2022 / Published online: 14 July 2022
© The Author(s), under exclusive licence to Springer Nature B.V. 2022

Abstract
This work focuses on the optical properties of single- and double-layer amorphous silicon nitride (a-SiN_x:H) thin films of different stoichiometry relevant for photovoltaic applications using PECVD technique. It is observed that the double layer SiN_x shows better anti-reflection property over a wide range of wavelengths than a single layer. Furthermore, it is shown that the films deposited under appropriately selected processing conditions contain hydrogen, as confirmed by Fourier-transform infrared spectroscopy. Minority carrier lifetime measurement and short circuit current density (J_{sc}) values for as-deposited single-and-double layer a-SiN_x:H are also investigated. The observed carrier lifetime, J_{sc} values and enhanced efficiency (an increment of ~21% with respect to the bare solar cell) shows that the a-SiN_x:H double layer would achieve high absorptivity in various optoelectronic devices and hence is a promising antireflection coating for solar cells.

Keywords Solar cell · Double layer silicon nitride · Minority carrier lifetime · Anti-reflection coating

1 Introduction

The silicon nitride (SiN_x) thin films of different stoichiometry have been extensively studied for their promising applications in photonic devices [1], creating optical filters [2], memory devices [3], membranes for micro-mechanical devices [4], gate dielectrics and isolation materials [5], and optical waveguides [6]. Growth of SiN_x thin films can be achieved using different techniques such as chemical vapor deposition (CVD), low-temperature-based plasma-enhanced CVD (PECVD), electron-cyclotron resonance plasma CVD, and sputtering techniques [7]. Low-temperature growth of SiN_x films is essential for many device applications, which is possible through PECVD processes. SiN_x film's properties can be tuned by controlling various parameters such as substrate temperature, deposition time, deposition pressure, reactants flow rate, and radio frequency power. In particular, the optical properties of SiN_x can be optimized as per the requirement by tuning the stoichiometry (x = [N]/[Si]) ratio [7]. This tunability of optical properties makes them excellent candidates for application in silicon solar cells, optoelectronic and microelectronic devices [8].

The single-layer anti-reflection coating (ARC) theoretically is only effective in the middle of the visible spectrum, i.e., 600 nm, whereas further reduction in reflectance in a broader wavelength range is possible in an optimally designed double-layer [9–12]. Recently, Sharma et al. reported that low weighted reflectance could be achieved by applying SiO2/TiO2 double-layer ARC on the front active surface to improve the efficiency of a photovoltaic cell. A gain in short circuit current (I_{sc}) from 2.18A to 3.32A, along with a gain in photovoltaic efficiency of about 14.34% compared to that of single-layer was reported in silicon solar cell [9]. The exploitation of different materials' combinations has been done as double-layer combination of different materials, which consists of SiO_2/TiO_2, MgF_2/ZnS, SiN/SiO_2, and MgF_2/CeO_2 [10, 11]. Almost all these double-layer anti-reflection coatings necessitate an intricate growth process and are not cost-effective. Multilayer SiN_x as ARC is promising due to the easy tunability of their optical properties with a change in stoichiometry. In addition, the insertion of the amorphous hydrogenated silicon nitride (a-SiN_x:H) layer reduces the number of interface states, reducing the likelihood of photogenerated carriers recombining at the a-SiN_x:H interface, facilitating photocurrent and photovoltage generation [12, 13]. A multilayer structure made up

✉ Pankaj Srivastava
pankajs@physics.iitd.ac.in

[1] Nanostech Laboratory, Department of Physics, Indian Institute of Technology Delhi, New Delhi 110016, India

of SiN_x layers of different stoichiometry will show refractive index contrast from one layer to the other. The greater refractive index of the a-SiN_x:H film results in higher optical absorption at shorter wavelengths, notably in the ultraviolet region of the solar spectrum, lowering the solar cells short-circuit current. [14, 15]. However, it is difficult to obtain desirable reflectance in a wide spectral region using a single layer.

We study the optical properties of single and double-layer a-SiN_x thin films of different stoichiometry in the present work. Minority carrier lifetime measurement is used to investigate the surface passivation behavior and anti-reflection capabilities of single-and-double layer a-SiN_x:H films. The refractive index of the reference single-layer (SL) film was chosen as 2.2, based on a typical equation in the literature [16, 17] that assumed a refractive index of 3.9 for silicon. The top layer of a double layer (DL) film usually has a low refractive index, while the bottom layer has a high one [18]. The top and bottom layers were made of a-SiN_x:H films with refractive indices of 2.2 and 2.9, respectively. Through ellipsometry, Fourier transform infrared (FTIR), and Raman spectroscopy, the optical band gap, refractive index, thickness, chemical bonding, and vibrational bonds of deposited thin films were analyzed. The optical properties were investigated by transmittance and reflectance characteristics for single- and double-layer films. The efficiency of Si-Solar cells after deposition of SL and DL coatings was compared with respect to a bare cell. The double-layer a-SiN_x:H film shows lower reflectance, higher minority carrier lifetime, J_{sc} values and improved efficiency, making it a promising choice for photovoltaic applications.

2 Materials and Methods

a-SiN_x:H thin films were grown on p-type Si substrates using the PECVD technique using SiH4 (4% in Ar) and NH_3 as precursor gases. The ratio of NH_3/SiH_4 is varied to grow silicon nitride films of different stoichiometry. Table 1 summarizes various parameters for the deposition of the films under study. The null ellipsometry at 632 nm was employed to determine the refractive index and thickness of as-deposited films. Spectroscopic ellipsometry was employed to obtain more precise thicknesses and optical and thermo-optical parameters of the layers. A Woollam Co., Inc, M-2000 J.A. RAE ellipsometer was used to take the measurements (rotating analyzer). The measurement of angles Ψ and Δ were done at an incidence angle of 70^0 within the spectral wavelength range of 300–1800 nm. The experimentally measured data is fitted with a Tauc Lorentz- and Cody Lorentz-type oscillator using the Complete EASE 6.0 software to find the optical constants. The mean-squared error (MSE) value was used to evaluate the degree of consistency between the model and the experimental data. The Shimadzu UV–VIS-NIR (Model: UV-3600) Spectrophotometer was used to record UV–Vis's spectra for as-deposited films. FTIR measurements were performed with a Bruker Vertex 70 vacuum spectrometer in transmission mode to determine the nature of chemical bonds present in the sample and quantify different bond species. Raman spectra were recorded in backscattering geometry using Raman spectroscopy (Renishaw in via RAMAN microscope) with 532 nm wavelength source. The short circuit current density (J_{sc} mA/cm^2) of as-deposited SL and DL films was measured experimentally. The photoconductance decay method (PCD) in the quasi-steady state photoconductance (QSSPC) mode was used to determine the effective carrier lifetime. In this work, the effective lifetime was measured in quasi-state modes using a commercial lifetime tester (WCT-120 Sinton Consulting, Inc.). The current–voltage (I-V) characteristics of the cells were recorded under illumination using a Class AAA solar simulator (Oriel Sol3A, Newport, USA) under standard one sun conditions (100 mW/cm^2, 25 °C).

3 Results and Discussion

The null ellipsometry results show that the increase in NH_3 flow rates decreases the index of refraction of as-deposited samples. The refractive index decreases from 2.9 to 2.0 for the samples A20 to A80, as tabulated in Table 1. The reduction in the refractive index indicates the change in stoichiometry towards Si_3N_4 with an increase in NH_3 flow rate. The double-layer film was fabricated by deposition of

Table 1 Deposition parameters, refractive index, thickness, and optical band gap of a-SiNx:H thin films. For all films, the rf power, deposition time and substrate temperature were kept as 50 W, 10 min, and 200 °C respectively

Sample	SiH_4 (4% in Ar) (sccm)	NH_3 (sccm)	Refractive index (@632 nm)	Thickness (nm)	Optical Band gap (E_g) (eV)
A20	1500	20	2.9	63	2.04
A40	1500	40	2.4	57	2.44
A60	1500	60	2.2	50	2.81
A80	1500	80	2.0	47	3.09

a non-stoichiometric a-SiN_x:H A60 (top layer) over A20 (bottom layer) film. The transmittance data for as-deposited films was recorded for films grown on the quartz substrate (not shown here). The bandgap information was extracted from the transmission data using Tauc's plot. It was evident from Tauc's plot that with an increase in NH_3 flow rate, the optical band gap also increases, which establishes compositional change from Si-rich to stoichiometric Si_3N_4 film. The calculated Tauc optical band gaps are tabulated in Table 1. For the double layer (DL) film, deposition parameters were kept the same as that of the single layer, except that those two layers (A60 as the top layer and A20 as the bottom layer) were deposited over each other, and their optical constants were extracted from spectroscopic ellipsometry.

Figure 1 shows the FTIR spectra in transmission mode of different a-SiN_x:H films deposited at various NH_3 gas flow rates. Generally, three groups of bonds like Si–N, N–H, and Si–H can be observed. The peak at 609 cm^{-1} is a Si–H wagging mode [19] due to hydrogen incorporation into the growing film from the source gases, SiH_4 and NH_3. The absorption peak detected at approximately 725 cm^{-1} is attributed to Si–N bonds symmetric stretching in amorphous Si_3N_4 [20, 21]. Si–N asymmetric stretching vibrational mode is observed around 850–900 cm^{-1}[22], whereas a peak between 1015–1080 cm^{-1} is the Si–O bond stretching mode [19] due to the oxidation of films. A broad feature due to N–H rocking vibration motion is observed around 1189 cm^{-1} [23]. Peaks in the above Fig. 1 around 2001 cm^{-1} and 2110 cm^{-1} are attributed to Si–H stretching vibrations. In a-SiN_x films, vibrational modes such as H–Si–Si_3, H–Si–HSi_2, H–Si–NSi_2, H–Si–SiN_2, H–Si–H, and H–Si–N_3 exist between 2000 and 2200 cm^{-1} [24].

Here, the position of N–H stretching vibration mode is at 3350 cm^{-1}[22]. With the NH_3 flow rate decreasing, the Si–H stretching bond and Si–N stretching bond increase, but the N–H stretching bond decreases due to more Si content in the film. The spectrum corresponding to the double layer is similar to single layer spectra.

As shown in Fig. 2, all Raman spectra show a dominant peak centred around 521 cm^{-1}, ascribed to the transverse optical (TO) mode of Si–Si vibrations in the crystalline phase [25]. The peak at 680 cm^{-1} corresponds to overtones of longitudinal acoustic phonon mode (LA), which might be caused by coordination defects resulting from hydrogen incorporation in films. The peak centred around 960 cm^{-1} is due to the transverse optical (TO) phonon [20]. In addition, the spectra indicate numerous Raman peaks from the presence of the β-Si_3N_4 mode. The Raman peaks at about 230 cm^{-1}, 620 cm^{-1} and 940 cm^{-1} are ascribed to β-Si_3N_4 and attributed to E_{2g} mode [25]. The broad peak around 920–1000 cm^{-1} is accredited to the presence of the Si–N bond. A peak centred around 950 cm^{-1} confirms the existence of ß-phase amorphous silicon nitride [21]. Raman study has confirmed the formation of amorphous silicon nitride. These measurements indicate that with the decrease in the flow rate of NH_3, the aggregation of Si nanoparticles improves. It may also allow unreacted Si atoms to form clusters in as-deposited films. Furthermore, two amorphous silicon regions, i.e., 300 cm^{-1} and 480 cm^{-1}, corresponding to the longitudinal acoustic mode (LA) and transverse optical mode (TO). The second order of the transverse acoustic (2TA) phonon mode is also responsible for the appearance of a weak peak at 430 cm^{-1}. Also, the intensity of this peak increases with a decrease in NH_3 flow.

The outputs of Spectroscopic Ellipsometry experiments are the ψ(λ) and Δ(λ) describing the function δ, the ratio of the p-polarized (r_p) and s-polarized (r_s) complex Fresnel reflection coefficients, as given by the equation reported in the literature [26]. In ellipsometry, measured data does not

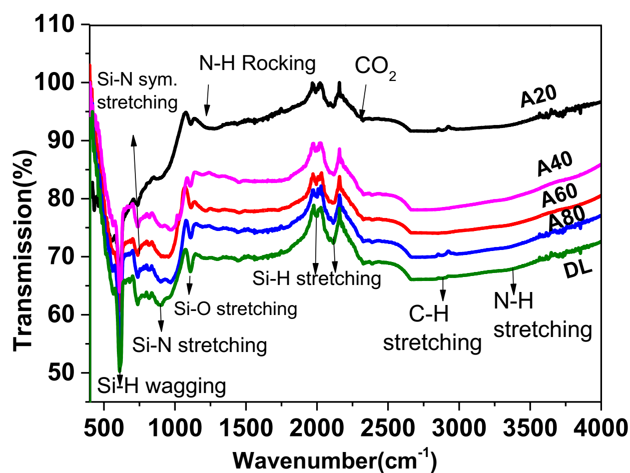

Fig. 1 All SiNx thin films with different stoichiometry have FTIR transmission spectra

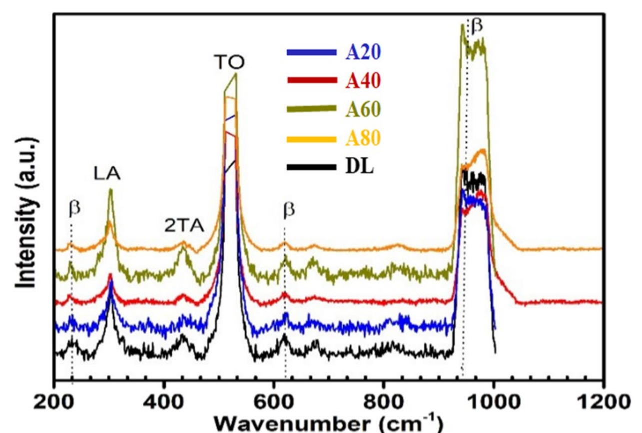

Fig. 2 Raman Spectra for different as-deposited samples with various refractive index

provide any information directly, instead, it must be modelled accurately to extract various characteristics such as refractive index/dielectric function, thickness, roughness, bandgap etc. The obtained experimental data of SL and DL samples are modeled with a bi- and tri-layer system composed of top silicon oxynitride (SiO_xN_y) and principal SiN_x layer on the Si substrate, as shown in Fig. 3. Due to atmospheric oxidation of a-SiN_x:H thin films, a SiO_xN_y layer is included in our model. The dangling bonds on the surface of a-SiN_x:H thin films should be saturated by this adsorbed layer [27]. The Kramers-Krönig relations are fitted to the acquired data to attain physical consistency between the real and imaginary components of optical constants like k(E) and n(E) [28–31]. The optical constants n and k are modeled with a Tauc Cody Lorentz and Tauc Lorentz-type oscillator model [32] by Complete EASE 6.0 software using optical models as depicted in Fig. 3. The results of fitting the optical models to the experimental data are shown in Fig. 4. The fitting parameters, MSE and optical parameters like refractive index (n) at 632 nm, bandgap (E_g), film thickness, oscillator strength/amplitude and peak energy for Lorentz oscillator (E_0) for all films are tabulated in Table 2. It provides valuable information on optical constants for the individual layers (Top-A60, Bottom-20) of DL film and all SL films.

Figure 5 depicts an experimental reflectance for SL and the DL films in 300–800 nm wavelength range. The reflection minima for A20, A40, A60 and A80 are at 754 nm, 508 nm, 440 nm, and 410 nm, respectively, whereas double-layer shows a broad reflectance minimum in the wide wavelength region. As we move from the near stoichiometry (A80; refractive index ~ 2.0) to Si-rich silicon nitride films, the reflection minima show a red-shift. This shift in reflection minima also affirms the variation in the refractive index of thin films [33].

It is evident from Fig. 5 that SL a-SiN_x:H films do not offer an excellent antireflection property for a wide wavelength range. On the other side, DL has a minimal reflection in the whole UV–visible region of the spectra, indicating potential antireflection property in the solar spectrum region. Double layer film shows the lowest average reflection percentage ~ 17% over an extended range of wavelength (300–800 nm) as the destructive interference condition is well satisfied, resulting in higher absorption of photons. The average reflection percent values are calculated for all deposited films in the 300–800 nm wavelength range and are shown in Table 3. This can be viewed from the reflection spectra that the antireflection effect of a DL film over a broad wavelength range is considerably superior to that of the SL. The broad reflectance minimum across the solar spectrum is generally the primary reason for higher light absorption and higher carrier generation [34, 35]. These improvements are represented by an increase in J_{sc}, τ_{eff} and a decrease in average reflectance percentage values, as shown in Fig. 6(b).

To investigate the effect of silicon passivation by a-SiN_x:H films, effective carrier lifetime in the silicon wafers is measured. The weighted average of the lifetime of carriers measured through the semiconductor material and surfaces is defined as an effective lifetime (τ_{eff}) given by Eq. (1):

$$\frac{1}{\tau_{eff}} = \frac{1}{\tau_{bulk}} + \frac{2S}{W} \tag{1}$$

where τ_{bulk} is the bulk lifetime of the material, S is the surface recombination velocity, and W is the thickness of silicon substrate. The photoconductance decay as a function of time is used to determine the lifetime. The quasi-steady-state photoconductance (QSSPC) established by Sinton [12] and transient photoconductance methods are commonly used for effective lifetime measurement. In transient and quasi-state modes, the effective lifetime was measured through a commercial lifetime tester (WCT-120 Sinton Consulting, Inc.). In most cases, the effective lifetimes are expressed by the equation given below [36]:

$$\tau_{eff}(\Delta n) = \frac{\Delta n(t)}{G(t) - \frac{d\Delta n(t)}{dt}} \tag{2}$$

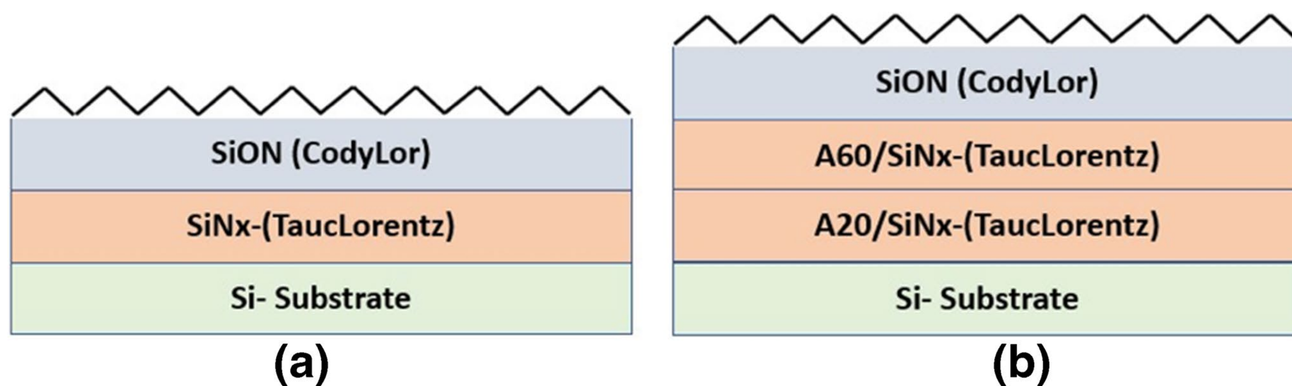

Fig. 3 Optical model of (**a**) single layer and (**b**) double layer used for experimental data fitting in spectroscopic ellipsometry

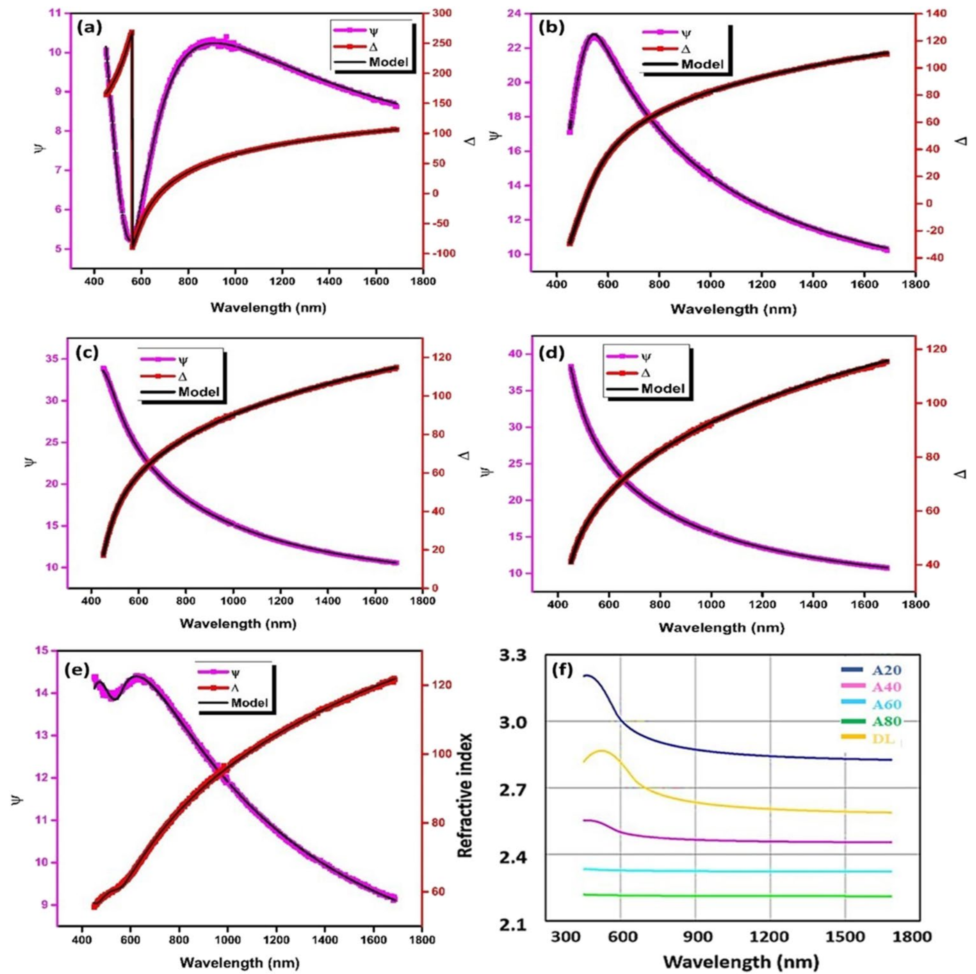

Fig. 4 Experimental and Model Generated Data Fits (**a**) A20 (**b**) A40 (**c**) A60 (**d**) A80 (**e**) DL (**f**) Refractive index v/s wavelength of all samples

Table 2 Fitting parameters, MSE and optical constants of all samples with variation in refractive index

	A20	A40	A60	A80	Top-A60 of DL	Bottom-A20 of DL
Thickness(nm)	65	53	48	48	17	20
E_g (eV)	2.0	2.2	2.4	2.6	2.5	2.1
n@632 nm	2.9	2.4	2.2	2.0	2.1	2.8
E_0 (eV)	5.1	6.6	4.9	7.2	5.4	2.1
Amplitude	233	168	98	103	441	218
MSE	1.9	1.8	1.7	1.4	1.7	1.7

where Δn is the injection level of carriers (electrons) and G is the generation of carriers. If Δn = Δp,

$$\Delta n(t) = \frac{\Delta\sigma(t)}{q\left(\mu_n + \mu_p\right)d} \quad (3)$$

where Δ σ(t) is a measured conductivity of the Si wafer as a function of time, d is the thickness of the Si wafer and μ_n and μ_p are mobilities of holes and electrons, respectively.

The conventional double layer silicon nitride film on silicon substrate may lead to enhancements in J_{sc} values of the designed structure via two cumulative effects, namely the passivation of the surface/bulk and the antireflection characteristic, which increases light absorption into the silicon substrate. With an increase in minority carrier density, changes in carrier inverse lifetime ($1/\tau_{eff}$) of single- and double-layer a-SiN_x:H films with varying refractive indices are shown

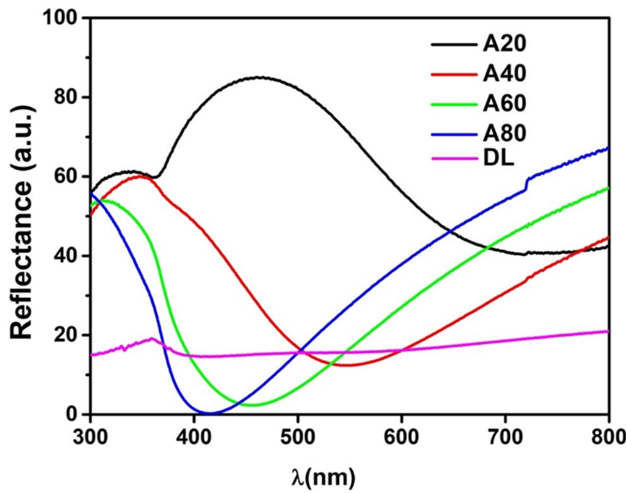

Fig. 5 Experimental reflectance percentage curve for different as deposited samples from A20 to DL

Table 3 Minority carrier lifetime, and average reflectance (%) at 300–800 nm of all as-deposited thin films

Sample	Average Reflectance (%) @(300-800 nm)	Minority carrier lifetime, effective τ (μsec) @ 10^{15} cm^{-3} density
A20	60.65	25.93
A40	32.59	15.13
A60	29.93	14.82
A80	34.38	20.34
DL	16.89	24.48

in Fig. 6(a). This can be seen from Eq. (1) that the τ_{eff} is dependent on the bulk minority carrier lifetime (τ_{bulk}) and the surface recombination velocity (S). τ_{eff} could be utilized as an indicator of the surface passivation quality if this is assumed that τ_{bulk} of all our measured samples has the same high lifetime values [12, 36, 37]. It is studied that the a-SiN_x:H films' passivation properties are influenced mainly by hydrogen content in the films [38, 39]. The effective minority lifetime measurement has been done for different excess minority carriers to get the best surface passivation quality out of all the samples. The maximum τ_{eff} occurred at an excess minority carrier ~ 1×10^{15} cm^{-3} is considered for passivation properties of all films. Table 3 demonstrates that when the a-SiN_x:H film's refractive index is 2.9, τ_{eff} is higher, indicating a low surface recombination velocity [36] and a high surface and bulk passivation effect compared to a structure with a a-SiN_x:H film of refractive index 2.2. As a result, the film with n = 2.9 was selected as the DL film's bottom layer. It should be observed that the transmittance of the n = 2.2 film was higher than that of the n = 2.9 film. As a result, the top layer for DL film was picked as the film with n = 2.2. It is evident from the Table 3 that DL film has a maximum τ_{eff} of ~ 25 μs in comparison to a single layer which has a maximum τ_{eff} of ~ 15 μs at a minority carrier density of ~ 1×10^{15} cm^{-3}. This implies that the DL film's surface and bulk passivation effect is superior to that of the SL film with the same material, which can be attributed to the DL film's higher hydrogen content [37, 39]. Compared to A60 single film, FTIR measurements reveal that the concentration of Si–H bonds and DL film's overall hydrogen bonding concentration is higher. The average interface trapped densities of DL film should be significantly low compared

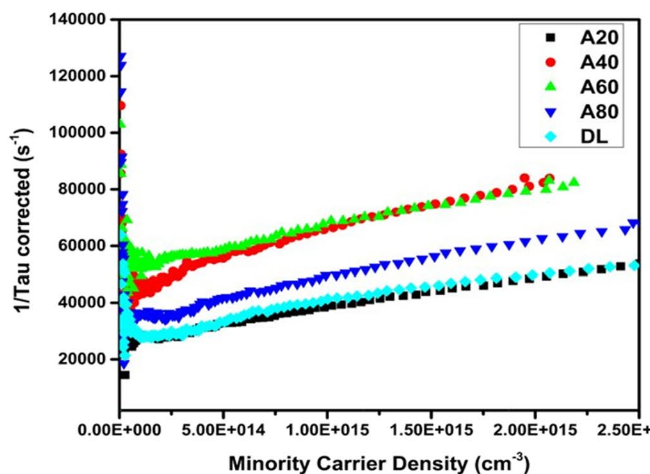

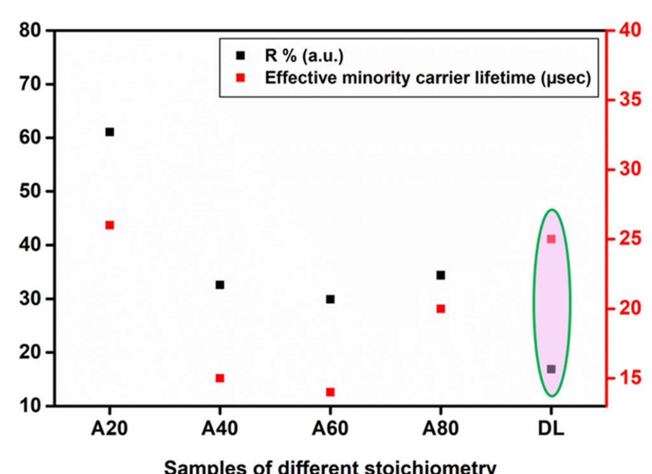

Fig. 6 **a** Measured inverse of effective minority carrier lifetimes (1/τ_{eff}) versus excess minority carrier density Δn for n-type silicon wafer with single/double layer SiNx deposited by PECVD. **b** Cumulative figure shows average reflectance (R%), and τ_{eff} (μs) values for all as-deposited different stoichiometric thin films

with single-layer film, which can improve surface passivation quality in DL film [12, 37]. It is ascribed to Si wafers with DL a-SiN_x:H film having a very low effective surface recombination compared to A60 single layer film deposited by PECVD for deposition temperature (T_d) = 200^{0}C.

Further, we have deposited the single-(A60) and the double-layer (DL) on bare Si-commercial solar cells to investigate changes in their overall efficiency. LIV curves obtained for different cells are shown in Fig. 7(a-c). It is more common to study the short-circuit current density (J_{sc} in mA/cm^2) rather than the short-circuit current to remove the area dependence of different cells. Various parameters such as short circuit current density (J_{sc}), open-circuit voltage (V_{oc}), fill factor (FF) and efficiency for solar cells coated with different a-SiN_x:H were calculated. Also, solar cell data obtained using the LIV curve are tabulated in Table 4. From the tabulated results, it is evident that both J_{sc} and V_{oc} values are minimum in the bare cell case compared to other films, resulting in the lowest FF and efficiency of the same. This may be attributed to the fact that the maximum incident light is reflected in the case of a bare cell in the solar spectrum range. A higher current density of 38.9 mA/cm^2 for the cell with DL compared to ~36.1 mA/cm^2 for a single cell with A60 single layer is observed, which can be accredited to the lesser DL film recombination rate and better anti-reflection characteristics [12, 33]. The increased J_{sc} value of the DL cell compared to the A60 single layer cell can be attributed to the DL cell's high transmittance, low reflectance (Fig. 5), and improved passivation effect (Fig. 6(a)), which makes it a good candidate for photovoltaic application. Also, from lifetime measurement, it is observed that τ_{eff} for DL film

Table 4 Solar Cell data for all cells with different a-SiNx:H coatings obtained using solar simulator

Sample	J_{sc} (mA/cm^2)	V_{oc} (mV)	FF	η(%)
Bare	33.5	586	0.73	14.5
A60 (Single Layer)	36.1	594	0.74	15.8
DL (Double Layer)	38.9	598	0.75	17.5

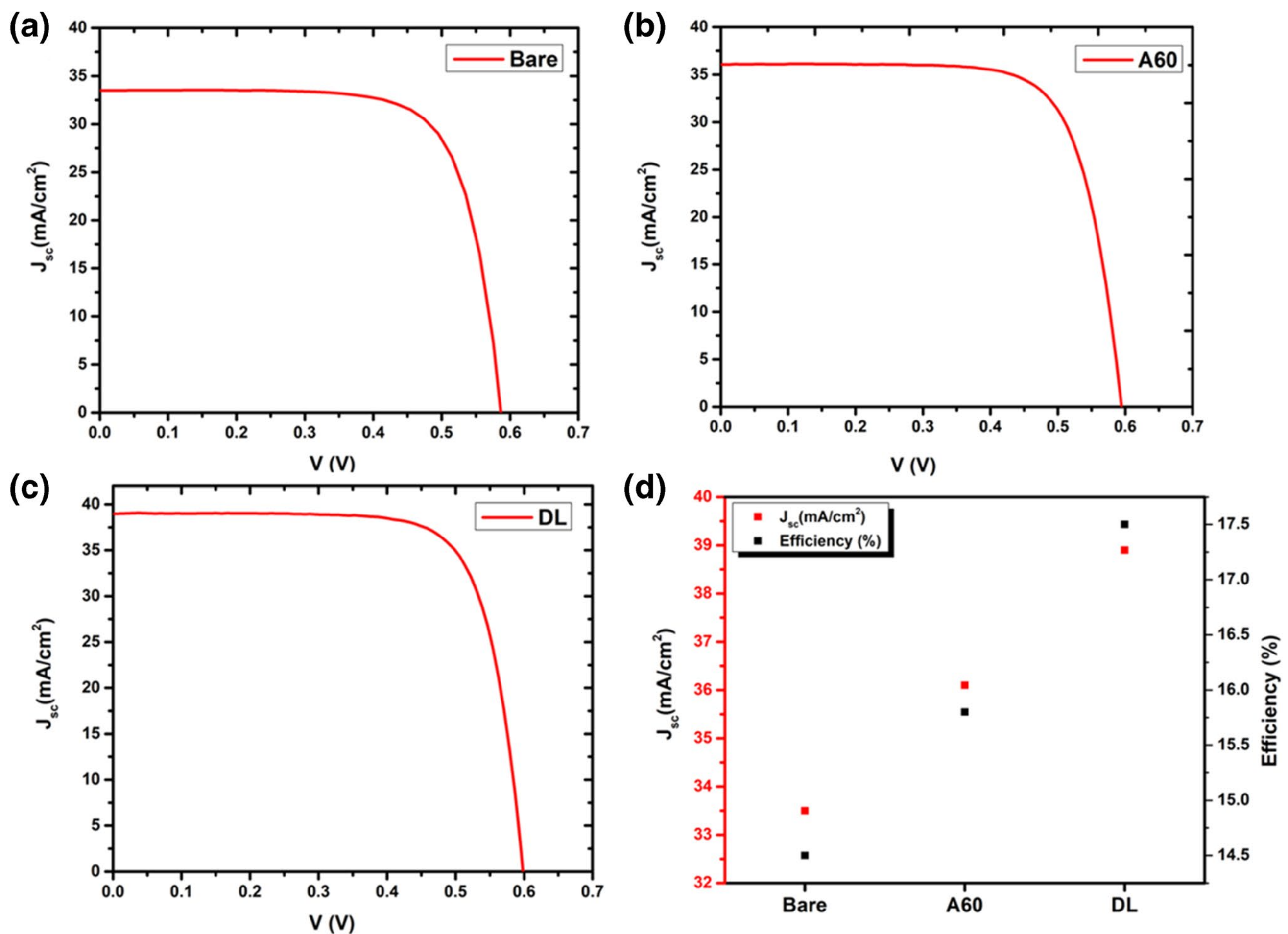

Fig.7 I-V characteristics under illumination (LIV): **a** bare cell; **b** A60; **c** DL; **d** Variation in efficiency, J_{sc} (mA/cm^2) of bare and coated solar cell with single (A60), double layer (DL) SiNx films

is higher than that of A60 single layer film owing to better surface and bulk passivation due to excess hydrogen in DL. Also, the product $J_{sc} \times V_{oc}$ is maximum for the DL, which improves the efficiency of DL coated cell, although J_{sc} is significantly higher in SL (A60) than that of the bare cell. Variations of efficiencies and short circuit current density (J_{sc}) for all the cells are shown in Fig. 7(d). In particular, a significant increase in solar cell efficiency is observed when bare Si-Solar cells are coated with SL (A60) and DL. Solar cell efficiency rises to 17.5% for the DL coated Si-solar cell, compared to 14.5%, obtained for the bare cell, i.e., an increment of ~ 21%.

It is anticipated that hydrogen continuously diffuses into the films and the underlying solar cell during deposition due to the applied growth temperature and reactive hydrogen radicals from the plasma. This results in an improved surface and bulk passivation of the solar cell and is reflected in an increment in the τ_{eff} and J_{sc} values. The passivation of the surface/bulk defects as suggested by carrier lifetime measurements and the antireflection characteristic, which increases light absorption into the solar cell, are two cumulative consequences of the traditional silicon nitride coating on solar cells. Hence, owing to its broader reflection minima and better minority carrier lifetime, DL is a good candidate for antireflection coating. Furthermore, several factors which lead to the highest efficiency of this cell are (i) the highest $J_{sc} \times V_{oc}$ value as discussed before, (ii) better passivation and antireflection properties and (iii) the highest fill factor. Hence, it can be concluded that the optical and electrical properties of the top DL layer are critical for enhancing solar cell efficiency.

4 Conclusions

Controlled growth and optimization of single and double layers of a-SiN_x:H thin films of different stoichiometries was achieved using PECVD. We see that single-layer coating is only effective as an anti-reflection coating in the middle of the visible spectrum (~ 600 nm). In contrast, DL film has lower overall reflectance in the broader wavelength range of 300–800 nm. Further, a bare commercial Si-solar cell was deposited with an SL (A60) and a DL of a-SiN_x:H thin films to investigate their efficiencies, J_{sc}, V_{oc} values and fill factor. The DL exhibited a significant effective lifetime (~ 25 µsec), higher J_{sc}, V_{oc} values and an enhanced efficiency. An increment of ~ 21% was achieved in the case of DL coated cell compared to the one coated with a single layer film. The present work suggests that a combination of more than one layer of the same material (e.g., a-Si_Nx:H) can be further exploited to reduce the optical losses to optimize the efficiency of silicon solar cells and optoelectronic Nano-devices.

Acknowledgements We thank Prof. Vamsi Krishna Komrala of IIT Delhi's Centre for Energy Studies for his assistance with minority carrier lifetime and solar cell efficiency measurements. The Nanoscale Research Facility (NRF), IIT Delhi is acknowledged for fabrication and optical measurements.

Author Contributions Pariksha Malik: Material Preparation, First Original Draft, Data collection, and Analysis; Harsh Gupta: Assisted in material deposition, analysis & data collection; Santanu Ghosh & Pankaj Srivastava: All authors have read, commented and approved the final manuscript.

Funding Financial support from Council of Scientific and Industrial Research (CSIR), New Delhi, India, as well as the fellowship provided by the University Grants Commission (UGC), New Delhi, India to author Pariksha Malik.

Data Availability Yes, the data are available.

Declarations

Ethics approval (Research involving human participants, their data or biological) material The Research is not involving the studies on human or their data.

Consent to participate Consent to participate.

Consent for Publication Consent for Publication.

Conflict of Interest No conflict of interest.

Competing Interest No conflict of interest.

References

1. Huang S, Arai K, Usami K, Oda S (2004) IEEE Trans Nanotechnol 3:210–214
2. Vernhes R, Zabeida O, Klemberg-Sapieha JE, Martinu L (2004) Appl Opt, AO 43:97–103
3. Yang MS, Cho KS, Jhe JH, Seo SY, Shin JH, Kim KJ, Moon DW (2004) Appl Phys Lett 85:3408–3410
4. Arora WJ, Nichol AJ, Smith HI, Barbastathis G (2006) Appl Phys Lett 88:053108
5. Misiakos I, Tsoi E, Halmagean E, Kakabakos S (1998) Monolithic integration of light emitting diodes, detectors and optical fibers on a silicon wafer: a CMOS compatible optical sensor. In: International Electron Devices Meeting 1998. Technical Digest (Cat. No. 98CH36217). IEEE, San Francisco, CA, USA, pp 25–28
6. Vohánka J, Ohlídal I, Ohlídal M, Šustek Š, Čermák M, Šulc V, Vašina P, Ženíšek J, Franta D (2019) Coatings 9:416
7. Vila M, Román E, Prieto C (2005) J Appl Phys 97:113710
8. Torchynska T, Polupan G, Khomenkova L, Slaoui A (2017) MRS Communications 7:280–285
9. Sharma R, Gupta A, Virdi D (2017) J Nano-Electron Phys 9:02001–02011
10. Rohatgi A, Chen Z, Doshi P, Pham T, Ruby D (1994) Appl Phys Lett 65:2087–2089
11. Jiao KL, Anderson WA (1987) Solar Cells 22:229–236
12. Lipiński M (2010) Arch Mater Sci Eng 46:69–87

13. Bommali RK, Ahmad S, Sharma N, Srivastava P, Prakash GV (2014) J Appl Phys 116:113501
14. Singh S, Park SH (2017) Indian J Pure Appl Phys 55:193–197
15 Stilhano Vilas Boas CR, Sturm JM, Bijkerk F (2019) J Appl Phys 126:155301
16. Green MA (1998) Solar cells: operating principles, technology and system applications. Kensington, NSW, Univ. of New South Wales
17. Liu Y, Ni L, Liu JB, Liu Q, Song C, Han G (2009) Surf Interface Anal 41:573–576
18. Lee I, Lim DG, Lee SH, Yi J (2001) Surf Coat Technol 137:86–91
19. Wolfe DM, Hinds BJ, Wang F, Lucovsky G, Ward BL, Xu M, Nemanich RJ, Maher DM (1999) J Vac Sci Technol A Vac Surf Films 17:2170–2177
20. Torchynska TV, Casas Espinola JL, Hernandez EV, Khomenkova L, Delachat F, Slaoui A (2015) Thin Solid Films 581:65–69
21. Muraki N, Katagiri G, Sergo V, Pezzotti G, Nishida T (1997) J Mater Sci 32:5419–5423
22. Bugaev K, Zelenina A, Volodin V (2012) Vibrational spectroscopy of chemical species in silicon and silicon-rich nitride thin films. Int J Spectrosc 2012:1155–1160. https://doi.org/10.1155/2012/281851
23. Gupta H, Bommali RK, Ghosh S, Srivastava P (2017) Nucl Instrum Methods Phys Res Sect B 410:164–170
24. Giorgis F, Giuliani F, Pirri CF, Tresso E, Summonte C, Rizzoli R, Galloni R, Desalvo A, Rava P (1998) Phil Mag B 77:925–944
25. Tiour F, Benyahia B, Brihi N, Sari A, Br M, Manseri A, Guenda A (2020) Appl Phys A 126:59
26. Singh SP, Srivastava P, Ghosh S, Khan SA, Prakash GV (2009) J Phys Condens Matter 21:095010
27. Bommali RK, Modi MH, Zhou S, Ghosh S, Srivastava P (2014) Appl Surf Sci 305:173–178
28. Fujiwara H (2003) Spectroscopic ellipsometry: principles and applications. John Wiley and Sons Ltd, Japan
29. Gupta H, Bommali RK, Ghosh S, Srivastava H, Srivastava A, Srivastava P (2021) J Appl Phys 129:035108
30. Bonneville DB, Miller JW, Smyth C, Mascher P, Bradley JDB (2021) Appl Sci 11:2110
31. Fujiwara H (2007) Spectroscopic ellipsometry: principles and applications. John Wiley and Sons Ltd, Japan
32. Cook C, Daly T, Liu R, Canonico M, Xie Q, Gregory RB, Zollner S (2004) Thin Solid Films 455–456:794–781
33. Braña AF, Gupta H, Bommali RK, Srivastava P, Ghosh S, Casero RP (2018) Thin Solid Films 662:21–26
34. Diaw A, Mbengue N, Diop MM, Ba O, Barro FI, Ba B (2016) Phys Mater Chem 3:37–39
35. Sahouane N, Zerga A (2014) Energy Procedia 44:118–125
36. Nagel H, Berge C, Aberle AG (1999) J Appl Phys 86:6218–6221
37. Cuevas A, Macdonald D (2004) Sol Energy 76:255–262
38. Y.L. Wang, Yu FTS, Sims VL, Brandhorst EW, Broder JD (1973) 10th IEEE Photovoltaic Specialists Conference:168–171
39. Kerr MJ, Cuevas A, Sinton RA (2002) J Appl Phys 91:399–404

Publisher's Note Springer Nature remains neutral with regard to jurisdictional claims in published maps and institutional affiliations.